Electronic Supplementary Material (ESI) for Sustainable Energy & Fuels.

Supporting information

Metal Organic Framework (MOF) derived Amorphous Nickel Boride: An electroactive material for electrochemical energy conversion and storage application

Rajat K. Tripathy, [a, b] Aneeya K. Samantara [a, b] and J. N. Behera [a, b*]

[a] *School of Chemical Sciences, National Institute of Science Education and Research (NISER), Bhubaneswar, P.O. Jatni, Khurda, Odisha-752050, India.*

[b] *Homi Bhabha National Institute(HBNI), Mumbai, India.*

*e-mail:jnbehera@niser.ac.in

Electrochemical calculations

The intrinsic electrochemical activity has been monitored by subtracting the solution resistance through iR compensation as per the following equation,

$$E_{iR\ corrected} = E_{observed} - iR \quad \text{..... (1)}$$

Here I and R are the experimental OER current and solution resistance respectively. The value of solution resistance has been obtained from the Nyquist EIS spectrum taken in a frequency range of 1 MHz to 0.1 Hz at an AC amplitude of 5 mV.

(a) Determination of Electrochemical active surface area (ECSA)

The electrochemical active surface area has been calculated by measuring the double layer capacitance (C_{dl}) of NiB, RuO_2, Ni-MOF and NiO. For this, CVs are collected in a non-Faradaic region (0.1-0.16 V vs. Hg/HgO) at different scan rates (5, 10, 25, 50, 100 mV/s). The average slope calculated from the plot of scan rate against cathodic and anodic peak current at 0.13 V (vs. Hg/HgO) gives the value of C_{dl} and then the ECSA has been calculated as per the following equation,

$$ECSA = \frac{C_{dl}}{C_s} \quad \text{..... (2)}$$

Here, C_s is the specific double layer capacitance of atomically smooth oxide surface in 1.0 M KOH electrolyte and its value is 0.04 mF/cm^2. Further the roughness factor (R_f) of the catalyst modified electrode are obtained by normalizing the ECSA with the geometrical surface area of the glassy carbon electrode.

(b) Turnover frequency (TOF)

Assuming that all the metal atoms are participating in the electrocatalysis process, the turn over frequency of NiB, RuO_2, Ni-MOF and NiO were calculated as per the following equation,

$$TOF = \frac{J \times S}{4F \times n} \quad \text{..... (3)}$$

J, S, F and n are the experimental OER current density, geometrical surface area of the working electrode, Faraday constant (96485.3 C/mol) and moles of active sites respectively. The value of n has been obtained by dividing the mass of sample loaded onto the electrode surface by molecular masses. Since four electrons ($4e^-$) are generated during the evolution of one mole of O_2, so the term 4 has been divided in the above equation.

(c) Calculation of specific capacitance, energy density and power density

The specific capacitance (C_s) of NiB has been calculated from both the cyclic voltammogram (equation 4) and galvanostatic charge-discharge profiles (equation 5) as per the following equations, [1,2]

$$C_s = \frac{\int_{V_a}^{V_c} I(V)dV}{m\vartheta\,(\Delta V)} \quad \ldots\ldots (4)$$

$$C_s = \frac{j}{slope} \quad \ldots\ldots (5)$$

Here, the $\int_{V_a}^{V_c} I(V)dV$, m, ϑ, (ΔV) are the integrated area of the CV curve, mass of the electrode material, scan rate and the optimized potential window taken for the measurement. "*j*" is the current density at which the galvanostatic charge-discharge (GCD) has been carried out and slope $\left({}^{\Delta v}/_{\Delta t}\right)$ has been obtained by linear fitting the discharge curve of the GCD profile. Thereafter the energy density (ED) and power density (PD) was calculated from the Cs values as per the following, [1–3]

$$ED = \frac{C_s(\Delta V)^2}{2} \quad \ldots\ldots (6)$$

$$PD = \frac{C_s(\Delta V)\vartheta}{2} \quad \ldots\ldots (7)$$

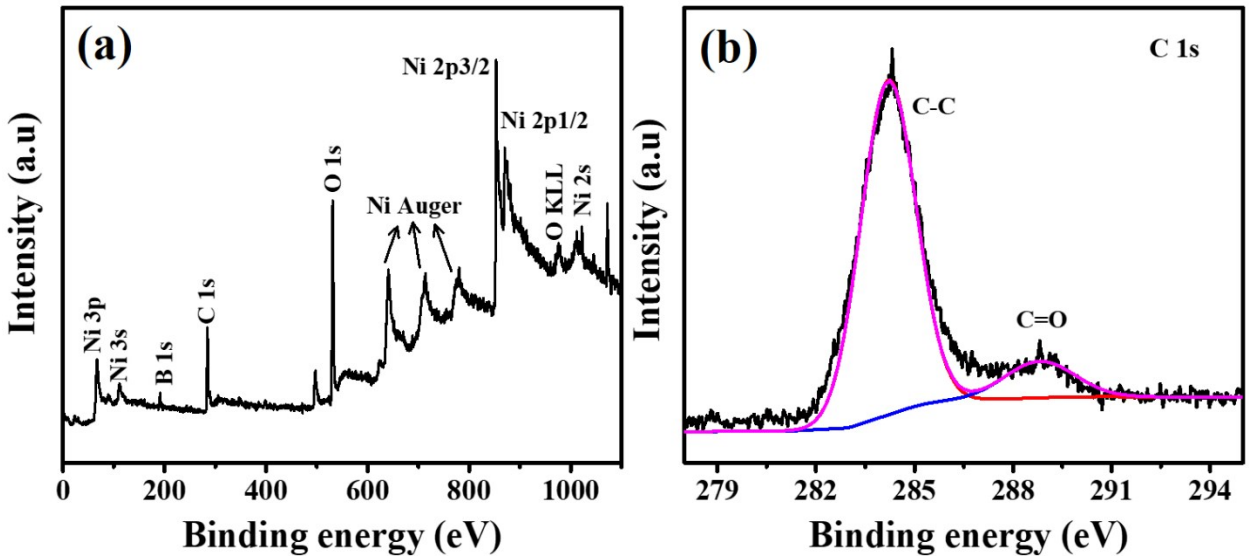

Fig. S1 (a) XPS survey spectrum of NiB and (b) high-resolution pattern of C1s of NiB.

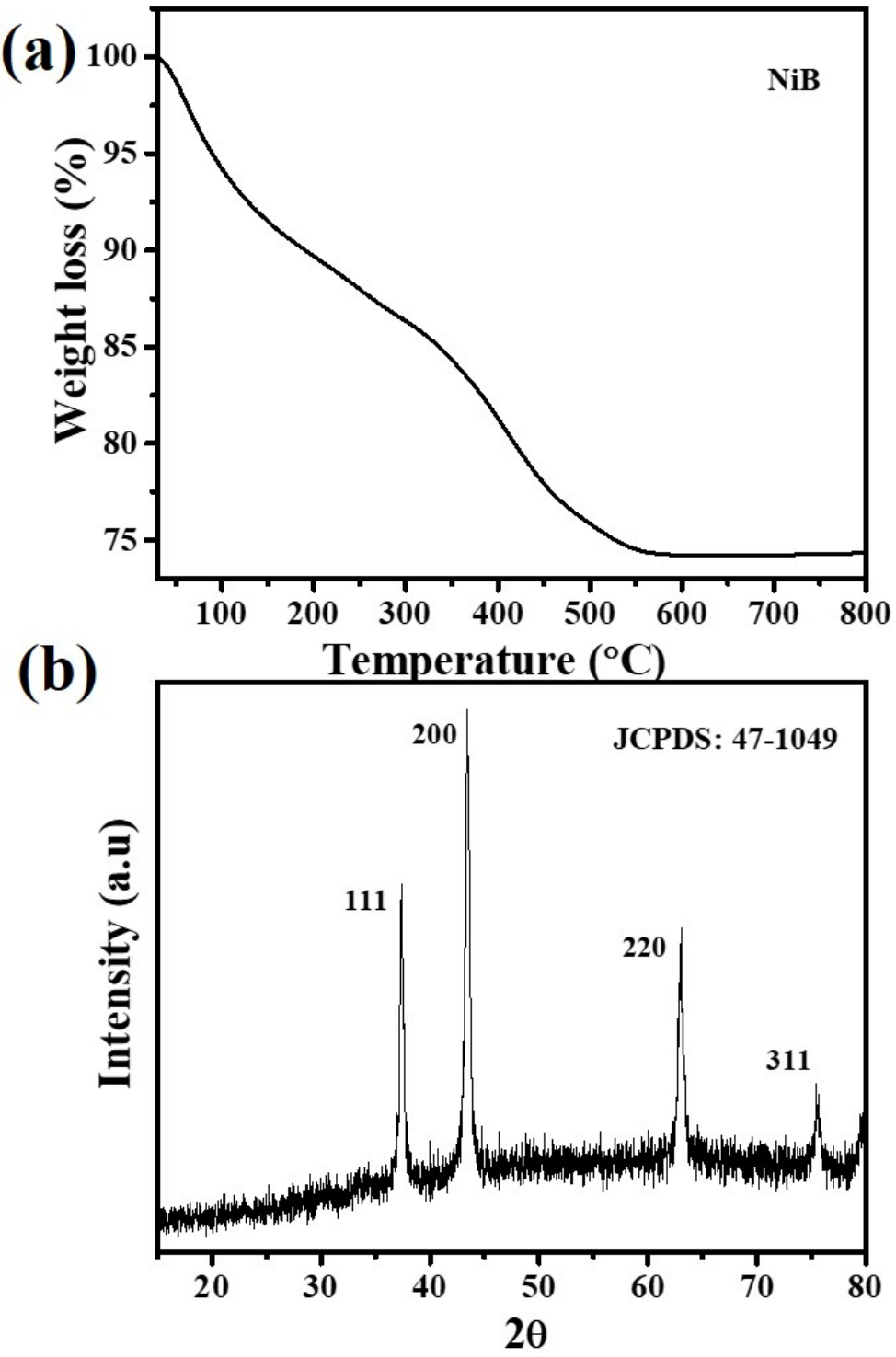

Fig. S2 (a) Thermogravimetric analysis and (b) powder X-ray diffraction pattern of post TGA NiB after 800 °C. The PXRD pattern well matched with the NiO (JCPDS: 47-1049).

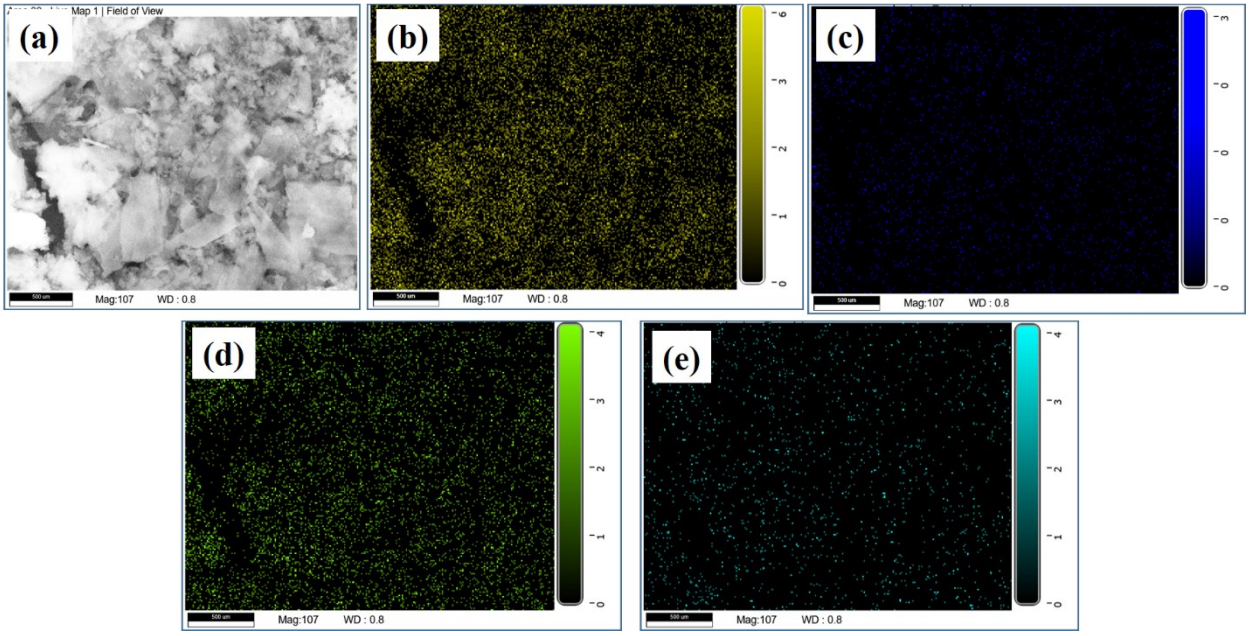

Fig. S3 Elemental mapping of Ni-MOF showing the (a) electron image and distribution of (b) carbon, (c) nitrogen, (d) oxygen and (e) Nickel elements.

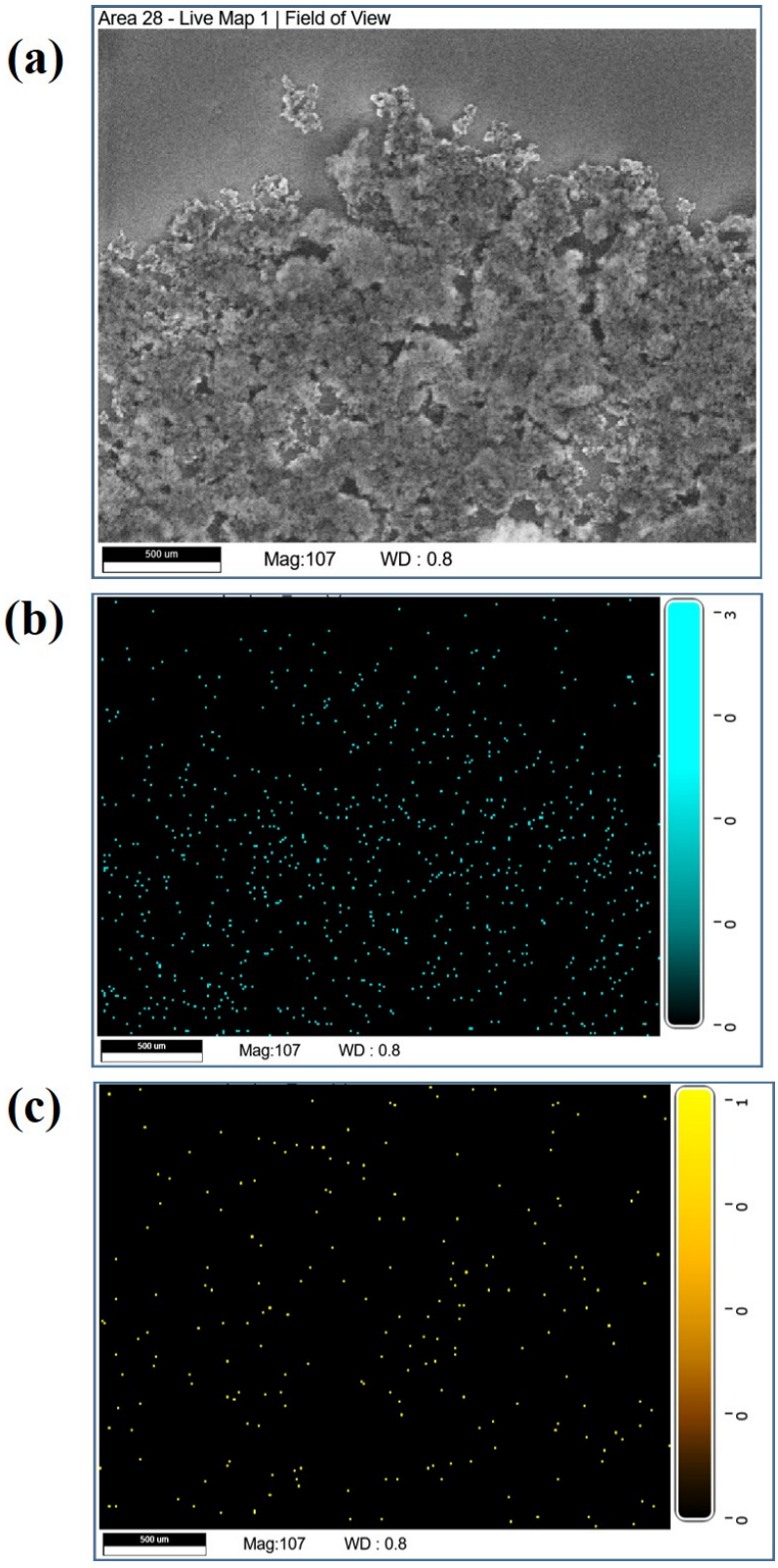

Fig. S4 Elemental mapping of NiB showing the (a) electron image and distribution of (b) Nickel and (c) boron elements.

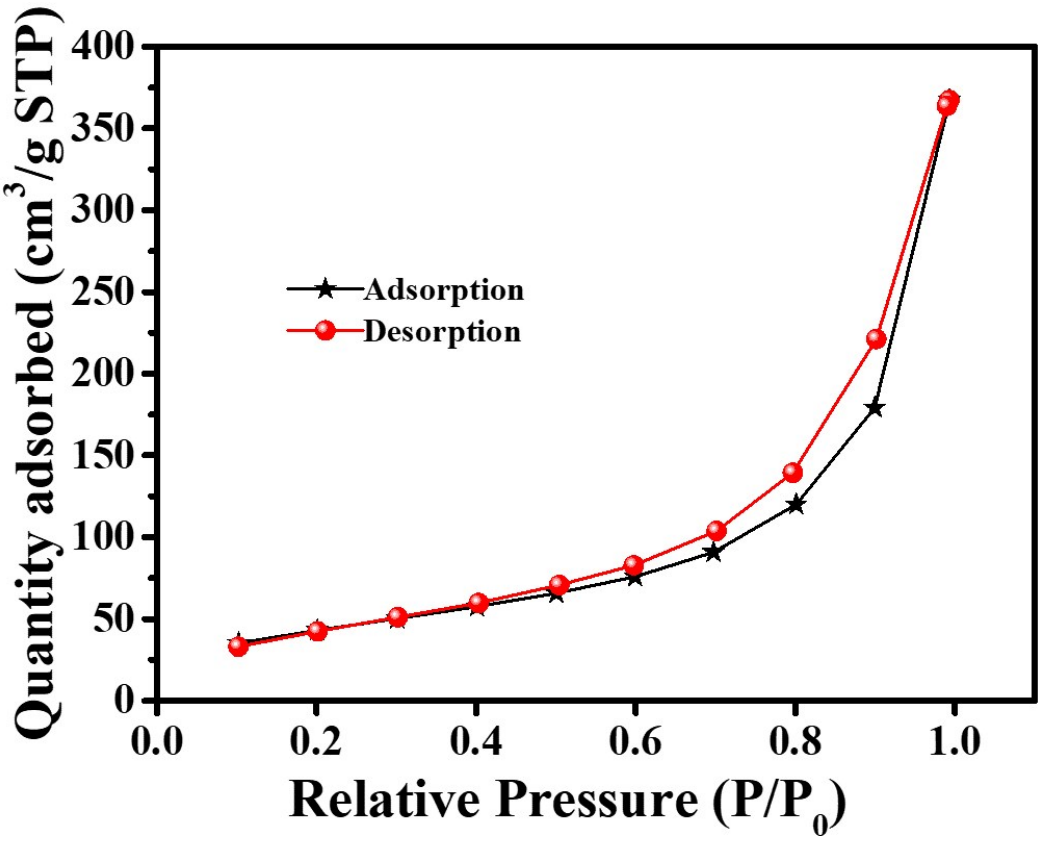

Fig. S5 Adsorption and desorption isotherms for nitrogen (at 77 K) of NiB

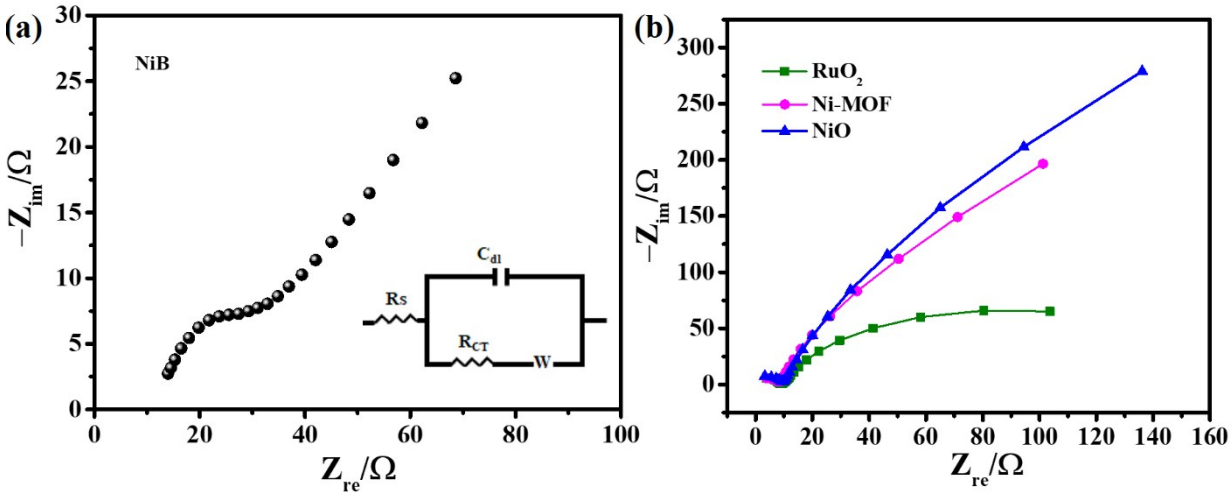

Fig. S6 Nyquist impedance spectrum of (a) NiB and (b) RuO_2, Ni-MOF and NiO in 1M KOH electrolyte.

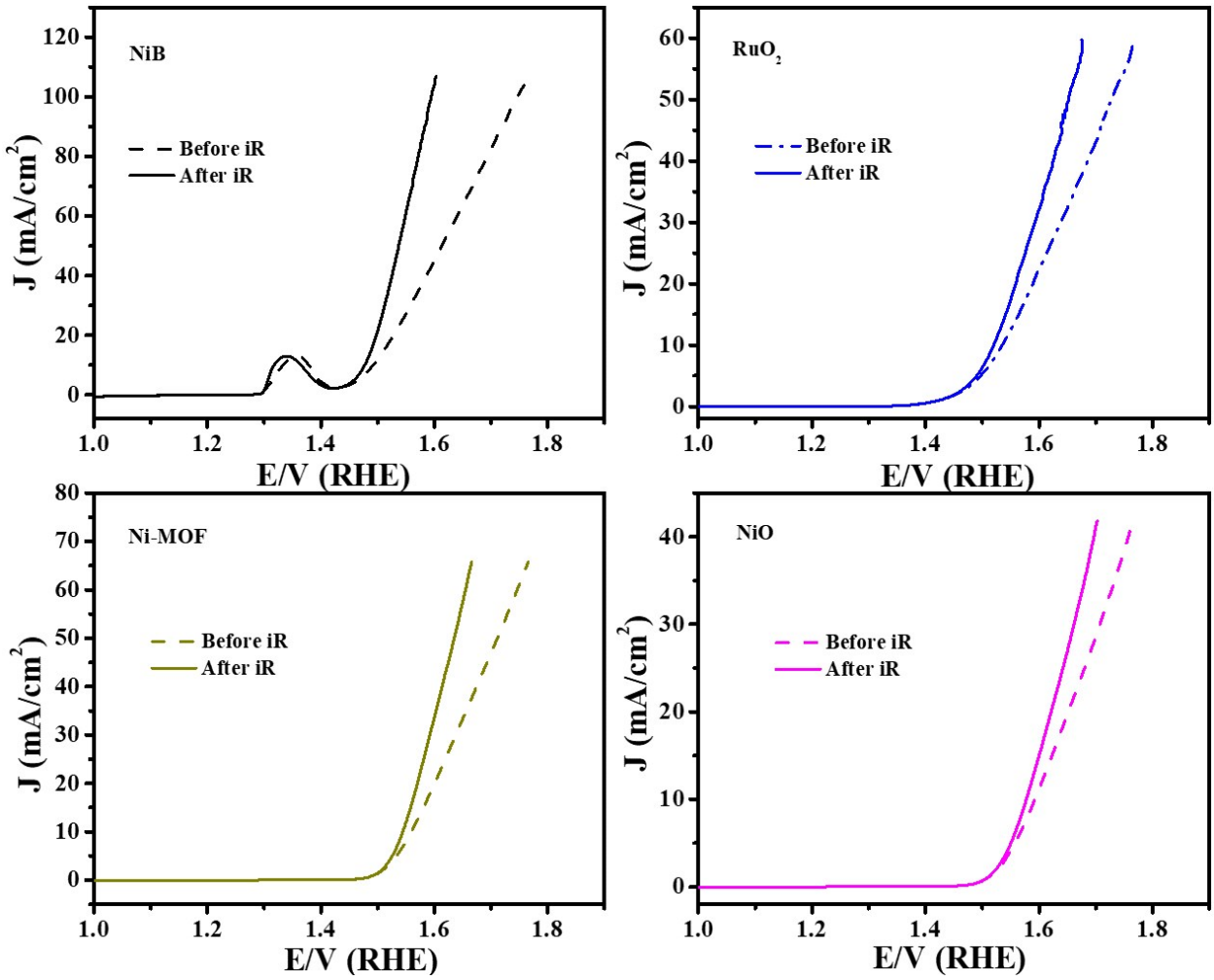

Fig. S7 OER polarization curve obtained with the NiB, RuO_2, Ni-MOF and NiO modified electrodes in 1.0 M KOH electrolyte at scan rate of 5 mV/s with and without iR-compensation.

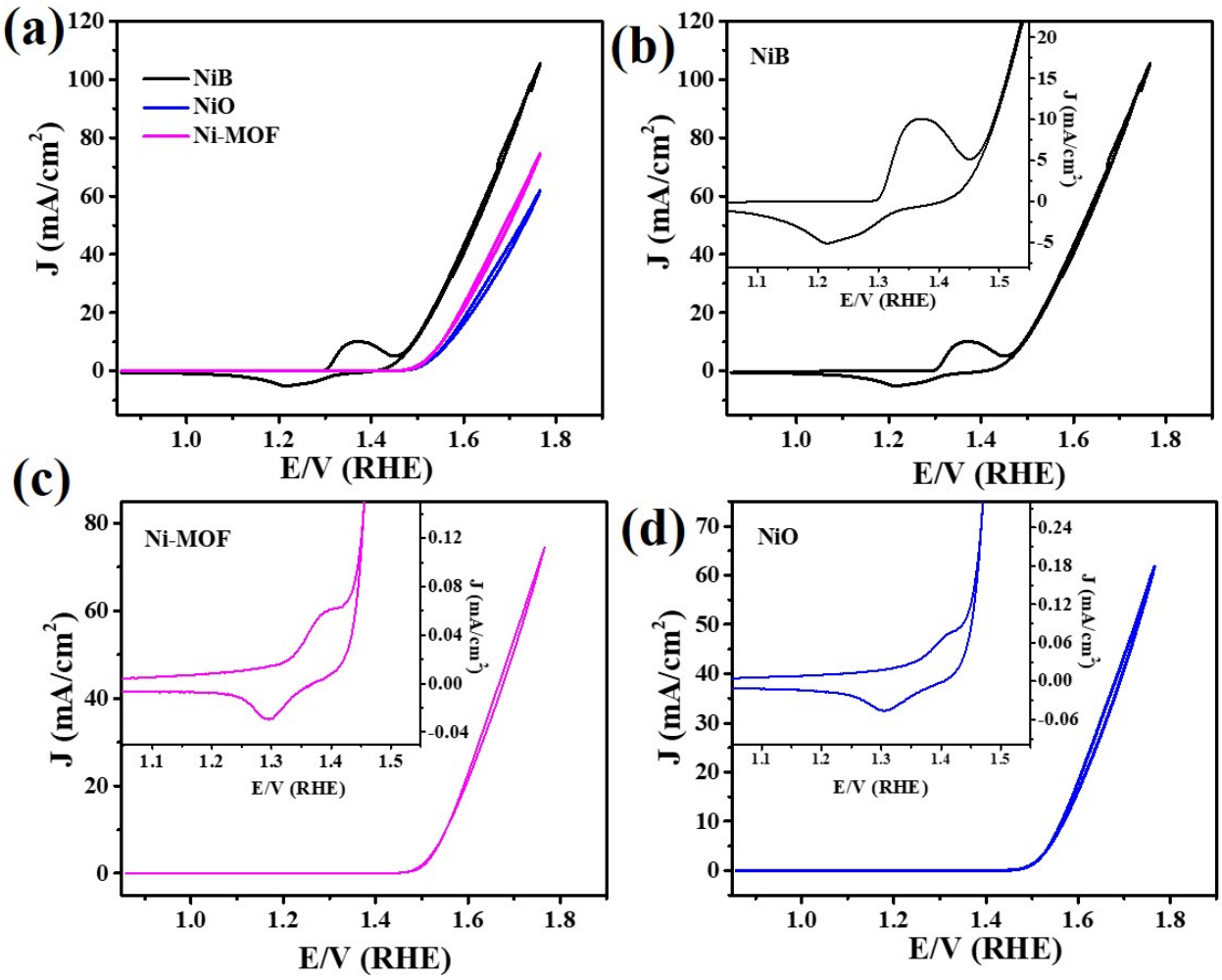

Fig. S8 Cyclic voltammograms of NiB, NiO and Ni-MOF at 5 mV/s scan rate in 1.0 M KOH electrolyte.

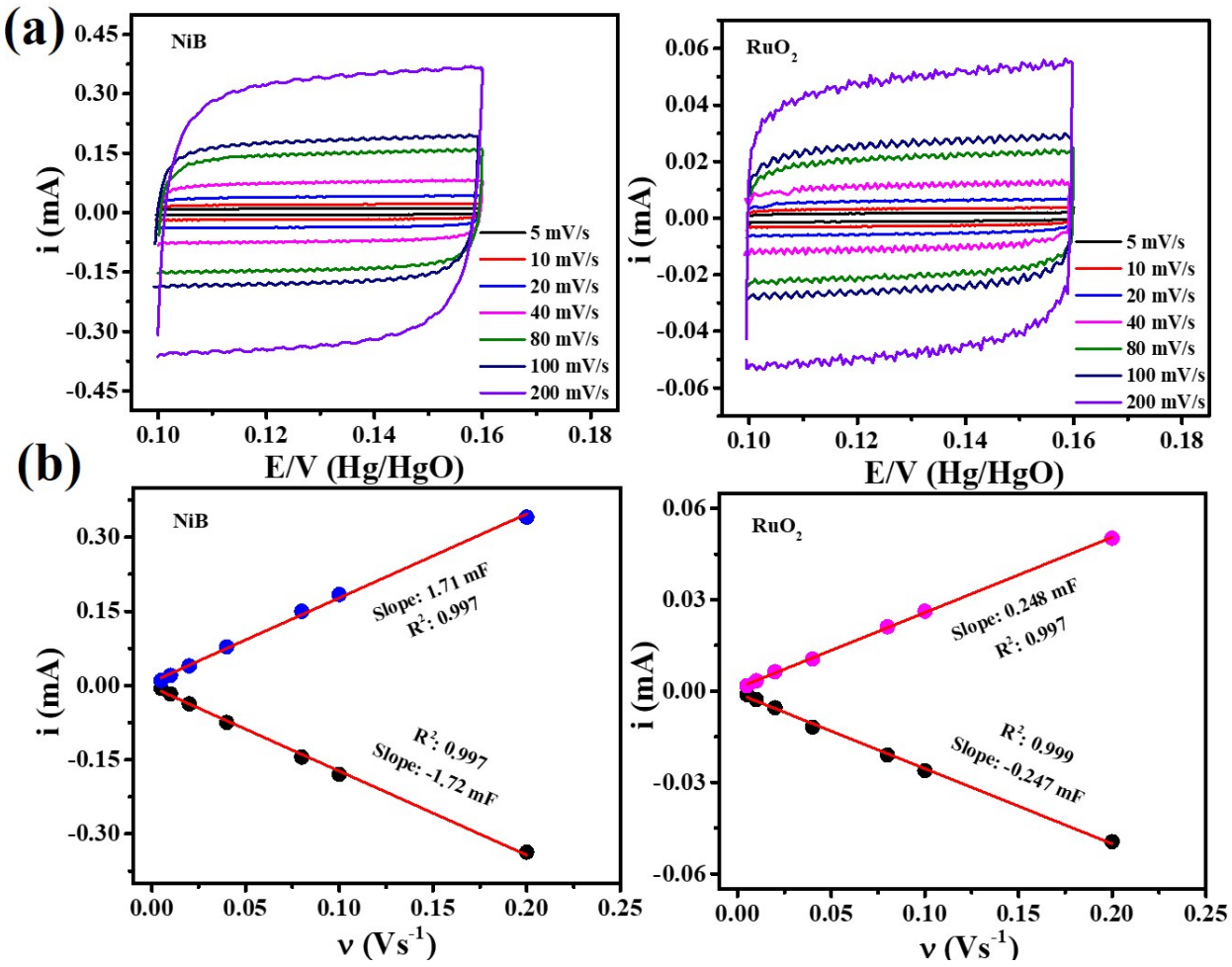

Fig. S9 (a) CV for NiB and RuO_2 showing the charging currents measured in a non-Faradaic region at a scan rate of 5, 10, 20, 40, 80, 100, 200 mV/s respectively and (b) the plot of cathodic and anodic charging currents measured at 0.13 V (vs. Hg/HgO) against scan rates.

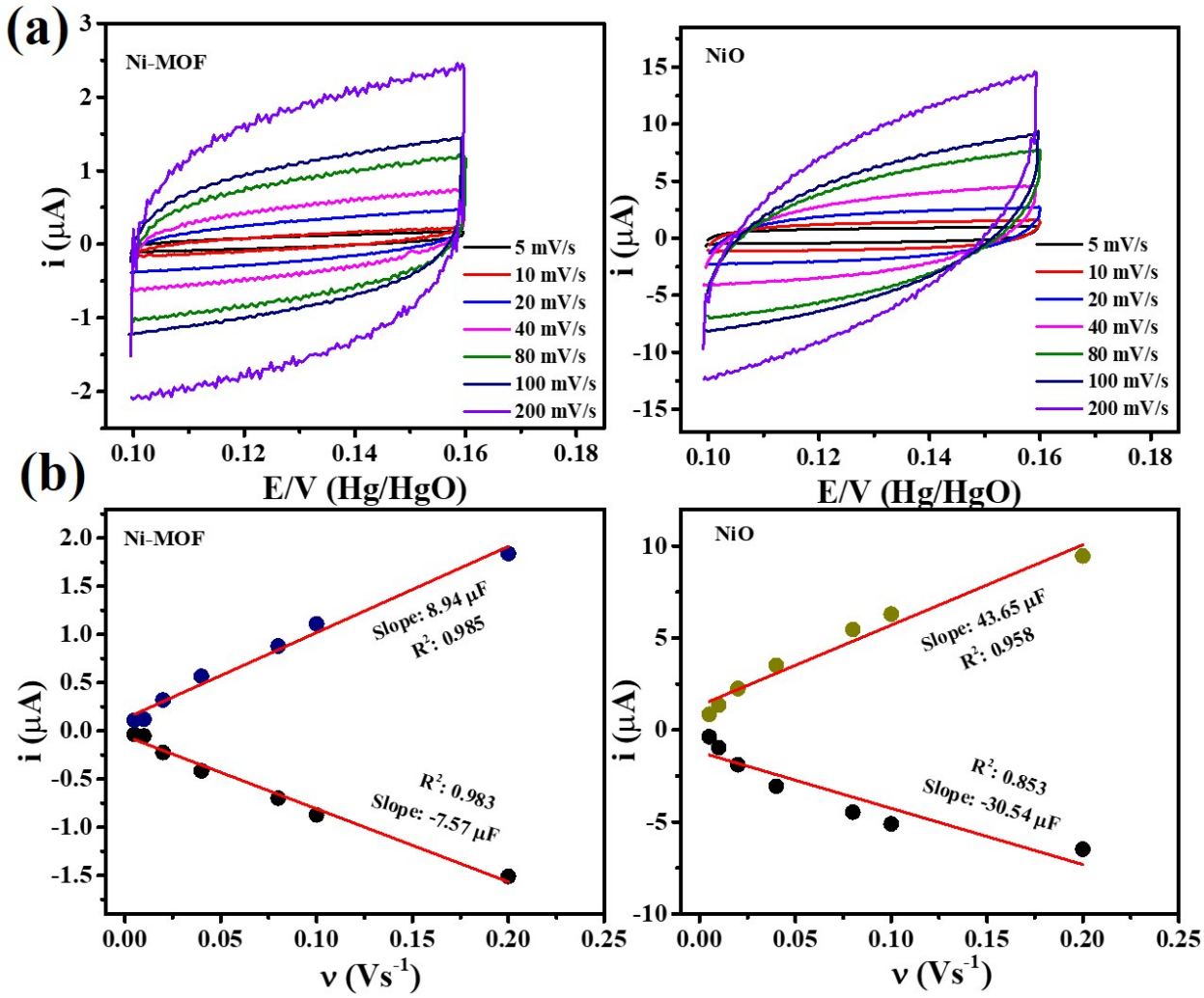

Fig. S10 (a) CV for Ni-MOF and NiO showing the charging currents measured in a non-Faradaic region at a scan rate of 5, 10, 20, 40, 80, 100, 200 mV/s respectively and (b) the plot of cathodic and anodic charging currents measured at 0.13 V (vs. Hg/HgO) against scan rates.

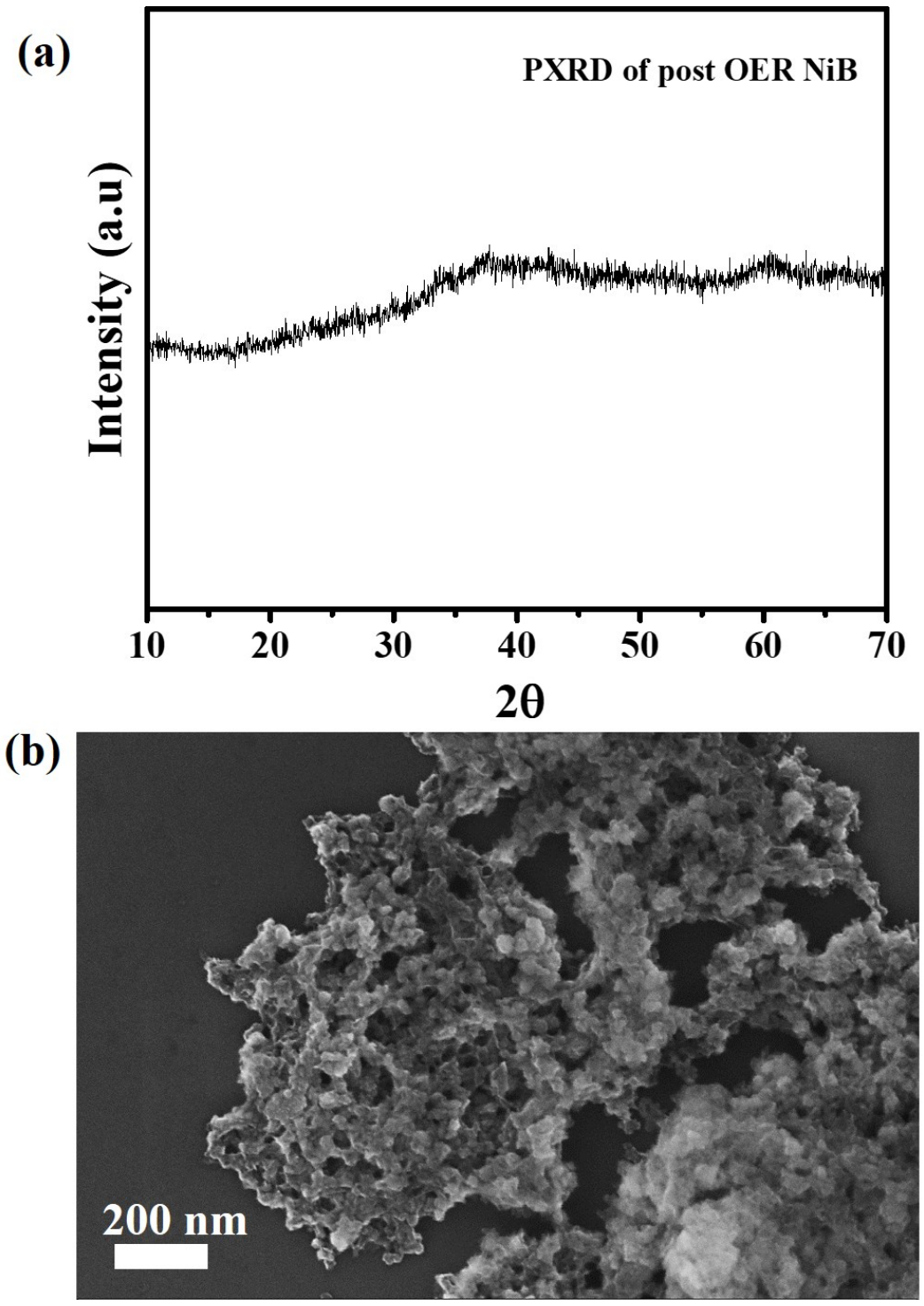

Fig. S11 (a) powder X-ray diffraction and (b) FESEM of post OER stability NiB.

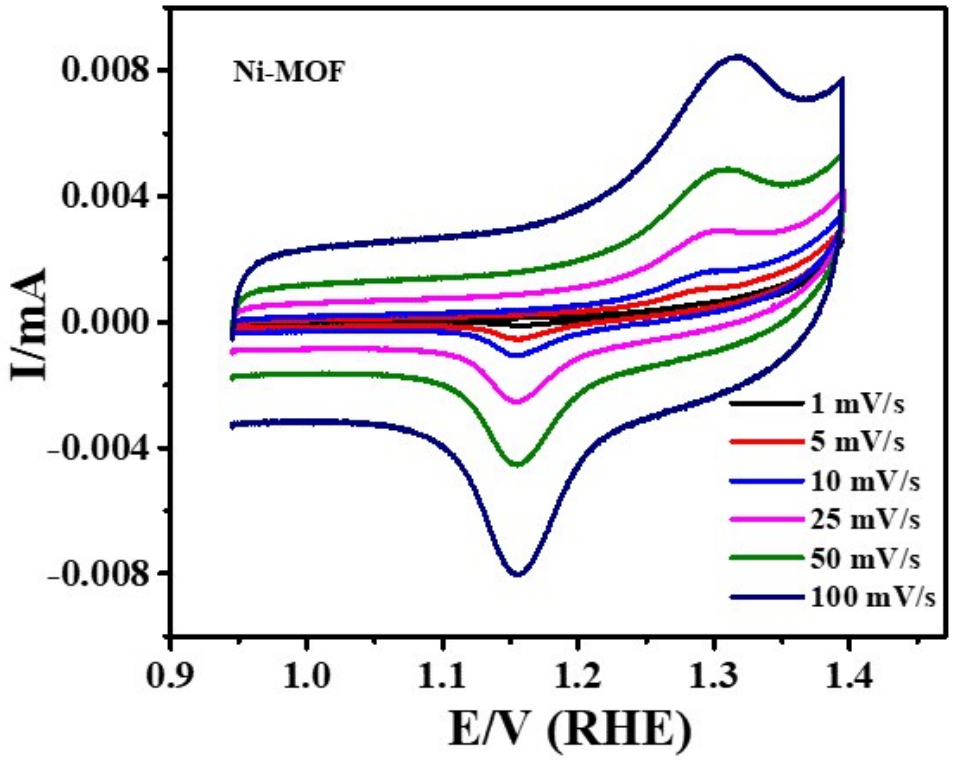

Fig. S12 Cyclic voltammogram of Ni-MOF modified electrode at different sweep rate in 5.0 M KOH electrolyte.

Calculation of capacitive contribution

At first the CVs of NiB modified electrode from 0.2 to 1.0 mV/s scan rate has been recorded (as Fig. S13) and found well preservation of the CV shape with increasing of scan rate. Thereafter the degree of capacitive effect has been calculated from the relation among the observed current (i) and scan rate (v) from the CV curves as per the following equation,

$$i = av^b$$

Here both the "a" and "b" are the constants and the value of "b" varies from 0.5 to 1.0 that calculated from the slope of the plot of *log i* vs. *log v* (Fig. S13 b).

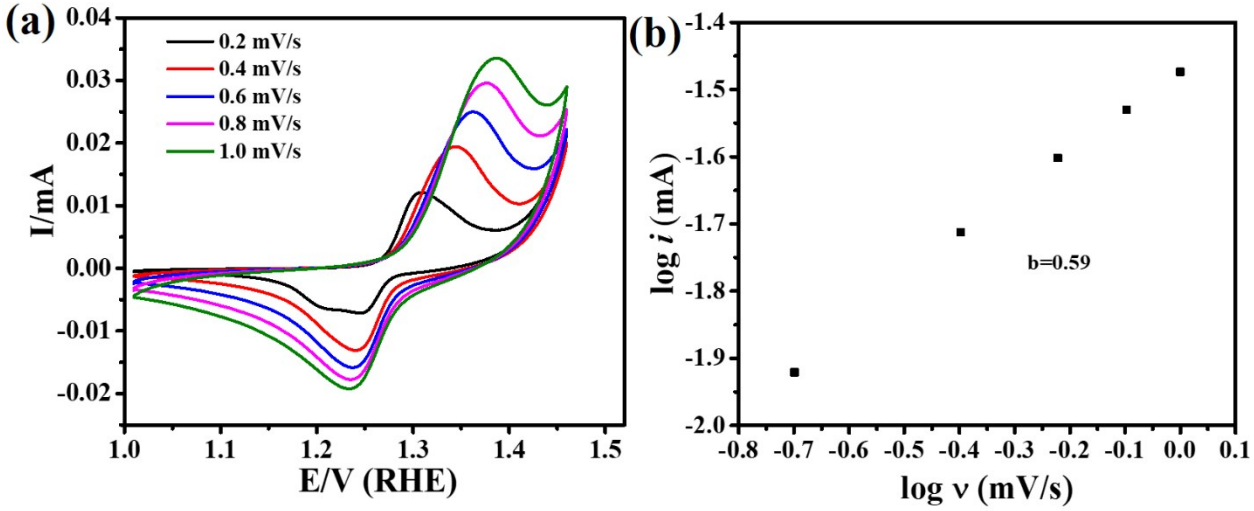

Fig. S13 (a) CV curves at various scan rates of NiB and (b) plot of logarithm of anodic peak current and logarithm of scan rate

As per the literature, for a diffusion controlled and surface capacitive process, the value of b approaches 0.5 and 1.0 respectively. [4,5] After getting the value of "b", the percentage of capacitive contribution to the current at a particular voltage has been determined quantitatively by separating the current response from the diffusion controlled and capacitive contribution at the corresponding voltage. Augustyn et al., and Chen et. al. was followed similar process to evaluate the charge storage contributions in their work. [6,7]

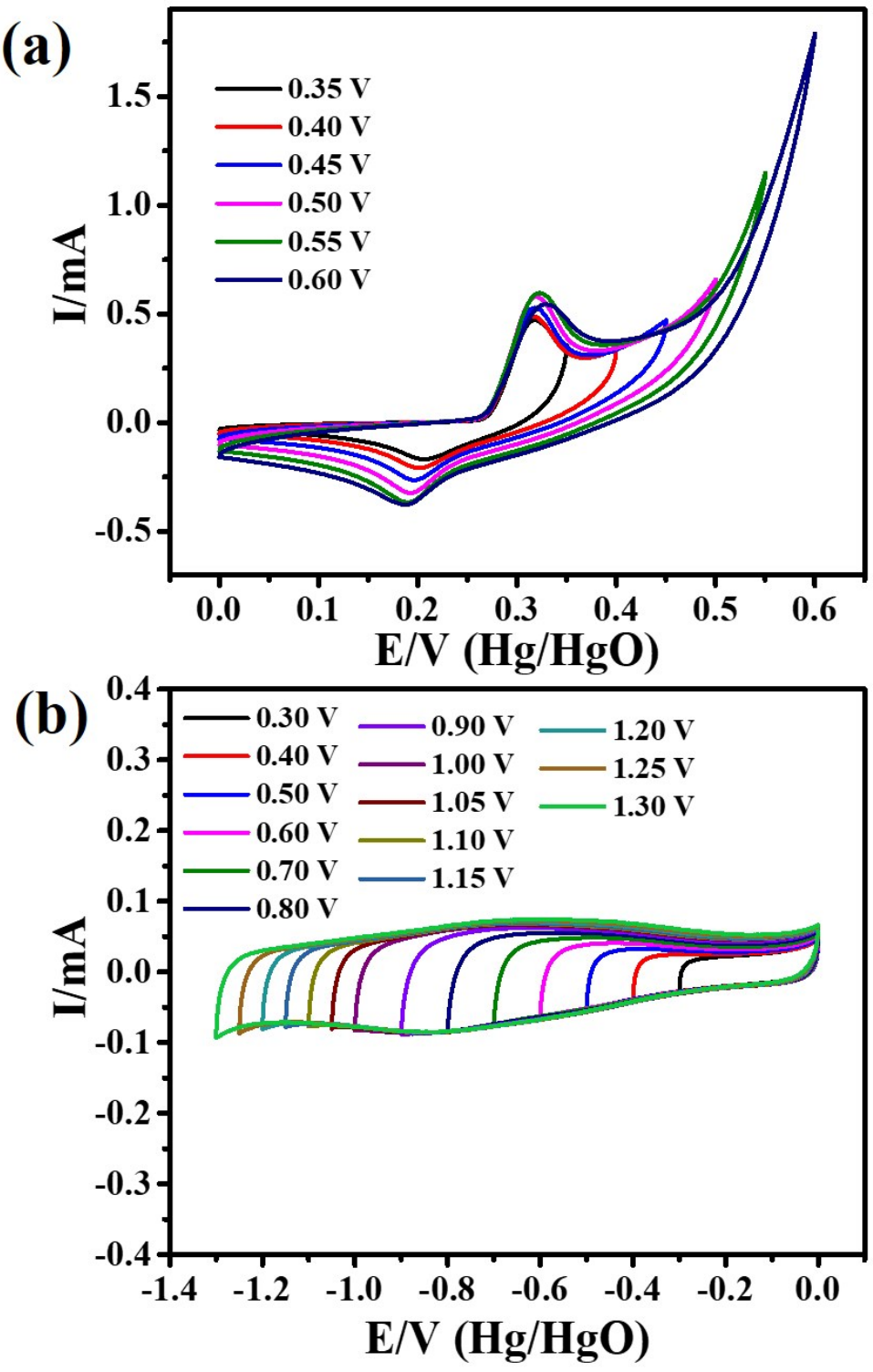

Fig. S14 Cyclic voltammograms showing the potential window optimization for the (a) NiB and (b) rGO in 5 M KOH electrolyte at a scan rate of 25 mV/s.

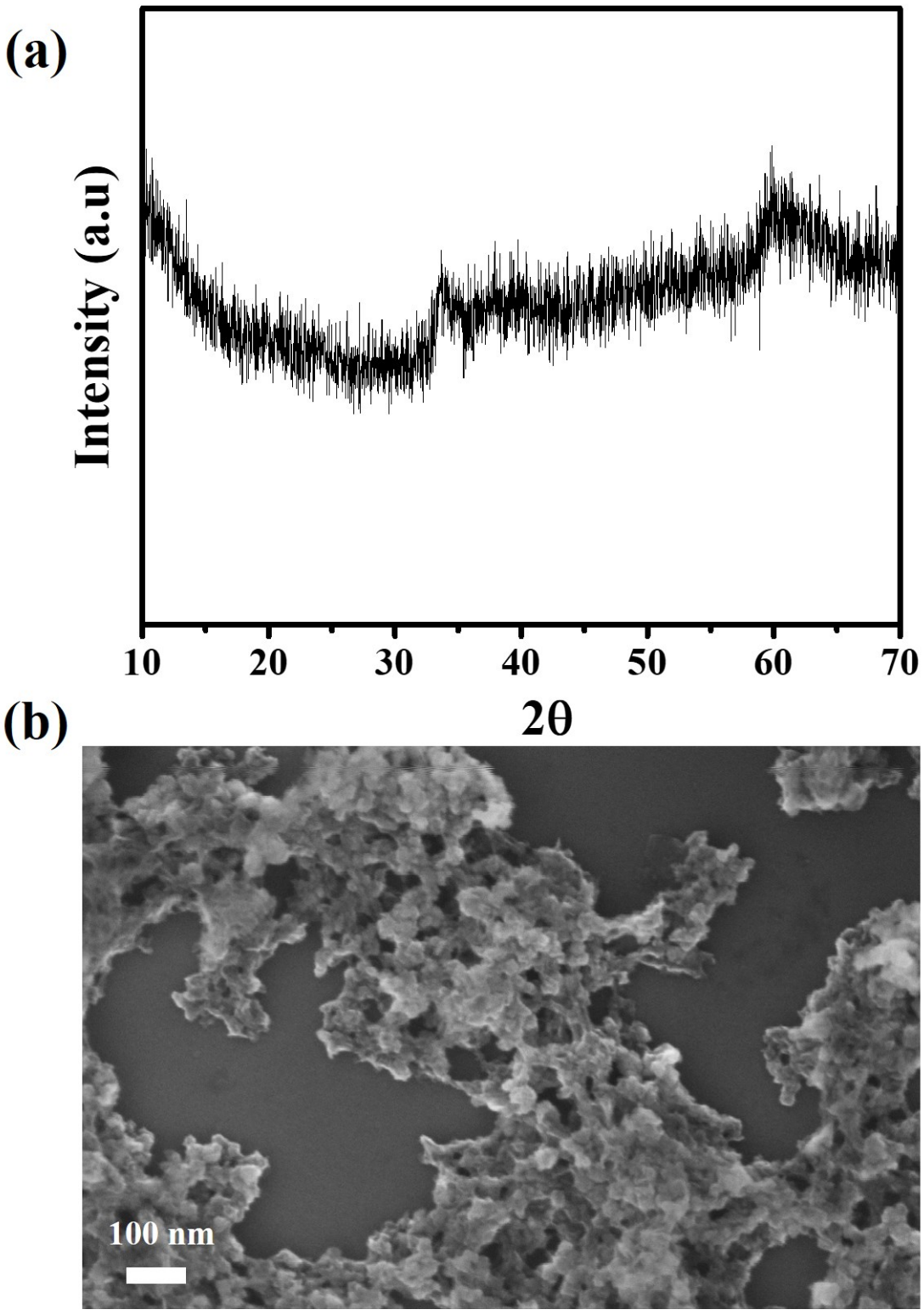

Fig. S15 (a) powder X-ray diffraction and (b) FESEM of post supercapacitor stability NiB.

Table S1 Electrocatalytic activity of different electrocatalyst

Catalysts	Electrolyte (Conc.)	Overpotential (mV) @10 mA/cm^{-2}	Tafel Slope (mV/dec)	References
Ni-Co-B	1M KOH	300	113	[8]
Ni_XB-300	1M KOH	380	89	[9]
Ni-B @ $Ni(OH)_2$ @ Ni foam	1M KOH	300@ 100mA/cm^{-2}	49.0	[10]
Ni-Fe-B/rGO	1M KOH	265	58	[11]
Ni_XB/f-MWCNT	1M KOH	286	46.3	[12]
Co-B/C	1M KOH	320	75.00	[13]
Co-B/NF	1M KOH	315	56.00	[14]
Co-3Mo-B	1M NaOH	320	155.0	[15]
Fe_2B	1M KOH	296	52.4	[16]
Fe_XB	1M KOH	260	57.9	[17]
Ni-B_i@NB	1M KOH	302	52.0	[18]
Ni-B-O @ Ni_3B	1M KOH	264	127.0	[19]
NiB	1 M KOH	240	58	Present work

Table S2 Table showing the OER activity of different electrocatalysts

	NiB	**RuO_2**	**Ni-MOF**	**NiO**
η@10 mA/cm^2 (mV)	240	290	310	350
Tafel Slope (mV/dec)	58	72	49	51
TOF (s^{-1})@η=240 mV	1.07	0.820	0.379	0.027
ECSA (cm^2)	42.875	6.187	0.21	0.927
R_f	225.66	32.56	1.08	4.88
MA@240 mV (A/g)	40	12.52	1.2	0.744

Table S3 Comparison of electrochemical charge storage performances of NiB with reported materials.

Sl. No.	Electrode material	Specific Capacitance (F/g)	Power Density (W/kg)	Energy density (Wh/kg)	References
1	Ni-Co-B	2226.96	788.91	66.40	[20]
2	Co-Ni/Boride/ Sulfide	1281	857.7	50.0	[21]
3	$Ni_{0.33}Co_{0.67}$)Se2	827.9	800.0	291.0	[22]
4	Ni/Co-MOF/rGO	860.0	42.5 kW/Kg	72.8	[23]
5	Ni/Co-MOF-5 derived Ni–Co–S	1377.5	1066.42	36.9	[24]
6	Zn-Co-S	1266	-	-	[25]
7	Mo-doped CoS HNC	781.0	799.9	27.7	[26]
8	NiB	2580.0	33.43 kW/kg	72.55	Present work

References:

1 S. Sahoo and C. S. Rout, *Electrochim. Acta*, 2016, **220**, 57–66.

2 A. Pathak, A. S. Gangan, S. Ratha, B. Chakraborty and C. S. Rout, *J. Phys. Chem. C*, 2017, **121**, 18992–19001.

3 S. M. Dinara, A. K. Samantara, J. K. Das, J. N. Behera, S. K. Nayak, D. J. Late and C. S. Rout, *Dalton Trans.*, 2019, **48**, 16873–16881.

4 G. A. Muller, J. B. Cook, H.-S. Kim, S. H. Tolbert and B. Dunn, *Nano Lett.*, 2015, **15**, 1911–1917.

5 A. J. Bard and L. R. Faulkner, *Fundamentals and Applications*, John Wiley & Sons, Ltd, New York, 1980, vol. 30.

6 C. Chen, Y. Wen, X. Hu, X. Ji, M. Yan, L. Mai, P. Hu, B. Shan and Y. Huang, *Nat. Commun.*, 2015, **6**, 6929.

7 V. Augustyn, J. Come, M. A. Lowe, J. W. Kim, P.-L. Taberna, S. H. Tolbert, H. D. Abruña, P. Simon and B. Dunn, *Nat. Mater.*, 2013, **12**, 518–522.

8 S. Wang, P. He, Z. Xie, L. Jia, M. He, X. Zhang, F. Dong, H. Liu, Y. Zhang and C. Li,

Electrochim. Acta, 2019, **296**, 644–652.

9 J. Masa, I. Sinev, H. Mistry, E. Ventosa, M. de la Mata, J. Arbiol, M. Muhler, B. Roldan Cuenya and W. Schuhmann, *Adv. Energy Mater.*, 2017, **7**, 1700381.

10 X. Liang, R. Dong, D. Li, X. Bu, F. Li, L. Shu, R. Wei and J. C. Ho, *Chem Cat Chem*, 2018, **10**, 4555–4561.

11 L. An, Y. Sun, Y. Zong, Q. Liu, J. Guo and X. Zhang, *J. Solid State Chem.*, 2018, **265**, 135–139.

12 X. Chen, Z. Yu, L. Wei, Z. Zhou, S. Zhai, J. Chen, Y. Wang, Q. Huang, H. E. Karahan, X. Liao and Y. Chen, *J. Mater. Chem. A*, 2019, **7**, 764–774.

13 Y. Li, H. Xu, H. Huang, L. Gao, Y. Zhao and T. Ma, *Electrochem. commun.*, 2018, **86**, 140–144.

14 Z. Chen, Q. Kang, G. Cao, N. Xu, H. Dai and P. Wang, *Int. J. Hydrogen Energy*, 2018, **43**, 6076–6087.

15 S. Gupta, N. Patel, R. Fernandes, S. Hanchate, A. Miotello and D. C. Kothari, *Electrochim. Acta*, 2017, **232**, 64–71.

16 H. Li, P. Wen, Q. Li, C. Dun, J. Xing, C. Lu, S. Adhikari, L. Jiang, D. L. Carroll and S. M. Geyer, *Adv. Energy Mater.*, 2017, **7**, 1700513.

17 L. Wang, J. Li, X. Zhao, W. Hao, X. Ma, S. Li and Y. Guo, *Adv. Mater. Interfaces*, 2019, **6**, 1801690.

18 W. J. Jiang, S. Niu, T. Tang, Q. H. Zhang, X. Z. Liu, Y. Zhang, Y. Y. Chen, J. H. Li, L. Gu, L. J. Wan and J. S. Hu, *Angew. Chemie - Int. Ed.*, 2017, **56**, 6572–6577.

19 W. Yuan, X. Zhao, W. Hao, J. Li, L. Wang, X. Ma and Y. Guo, *Chem Electro Chem*, 2019, **6**, 764–770.

20 R. Chen, L. Liu, J. Zhou, L. Hou and F. Gao, *J. Power Sources*, 2017, **341**, 75–82.

21 Q. Wang, Y. Luo, R. Hou, S. Zaman, K. Qi, H. Liu, H. S. Park and B. Y. Xia, *Adv. Mater.*, 2019, **31**, 1905744.

22 L. Quan, T. Liu, M. Yi, Q. Chen, D. Cai and H. Zhan, *Electrochim. Acta*, 2018, **281**, 109–116.

23 M. S. Rahmanifar, H. Hesari, A. Noori, M. Y. Masoomi, A. Morsali and M. F. Mousavi, *Electrochim. Acta*, 2018, **275**, 76–86.

24 C. Chen, M. K. Wu, K. Tao, J. J. Zhou, Y. L. Li, X. Han and L. Han, *Dalton Trans.*, 2018,

47, 5639–5645.

25 P. Zhang, B. Y. Guan, L. Yu and X. W. D. Lou, *Angew. Chemie*, 2017, **129**, 7247–7251.

26 Z. Yang, Q. Ma, L. Han and K. Tao, *Inorg. Chem. Front.*, 2019, **6**, 2178–2184.